



ELSEVIER

Contents lists available at SciVerse ScienceDirect

Earth and Planetary Science Letters

journal homepage: www.elsevier.com/locate/epsl

Strength evolution of a reactive frictional interface is controlled by the dynamics of contacts and chemical effects

François Renard^{a,b,*}, Sophie Beauprêtre^a, Christophe Voisin^a, Dimitri Zigone^a, Thibault Candela^{a,c}, Dag K. Dysthe^b, Jean-Pierre Gratier^a

^a ISTerre, University of Grenoble I, CNRS, BP 53, 38041 Grenoble, France

^b Physics of Geological Processes, University of Oslo, Norway

^c Department of Earth and Planetary Sciences, University of California–Santa Cruz, Santa Cruz, California 95064, USA

ARTICLE INFO

Article history:

Received 4 October 2011

Received in revised form

25 February 2012

Accepted 23 April 2012

Editor: L. Stixrude

Keywords:

fault

friction

healing

ABSTRACT

Assessing the healing rate of a fault is relevant to the knowledge of the seismic machinery. However, measuring fault healing at the depths where it occurs still remains inaccessible. We have designed an analog laboratory experiment of a simulated rough fault that undergoes healing and investigate the relative roles of interface chemical reactivity and sliding velocity on the healing rate. Slide-hold-slide experiments are conducted on a bare interface with various materials in contact (glass/glass, salt/glass, and salt/salt) with or without the presence of a reactive fluid and the slider-surface pull-off force is measured. Our results show that the interface strengthens with hold time, whatever the conditions of the experiments. In addition, we quantify the effect of chemical reactivity on the healing rate. Considering the glass/glass case as a reference, we show that the healing rate is increased by a factor of 2 for the salt/glass case; by a factor of 3 for the salt/salt case; and by about a factor of 20 when saturated brine is added on a salt/salt interface. We also measure that the sliding velocity affects the healing rate for salt/salt interfaces at room humidity. A careful optical monitoring of the interface allows a direct observation of the contact growth characteristics associated to each type of materials. Finally, the large differences of healing rate are interpreted through a mechanistic approach, where the various experimental conditions allow separating different healing mechanisms: increase of adhesion of the contacts by welding, contact growth due to creep or due to neck growth driven by surface tension.

© 2012 Elsevier B.V. All rights reserved.

1. Introduction

Immediately after an earthquake, a fault starts healing and strengthening. During the period between two major earthquakes, defined as the interseismic period, the fault may creep, compact, and seal, leading to a progressive increase of the mechanical strength of the fault zone (Li et al., 2003; Vidale and Li, 2003; Gratier et al., 2003). Such fault re-strengthening during interseismic periods can be measured from periodic or continuous records of seismic velocities variations in the damage zone surrounding large earthquakes (Li et al., 2003; Brenguier et al., 2008). It has been proposed that these variations may be related to the closure of partially fluid-filled cracks in the rupture zone and the recovery of microscopic damage; a behavior known as fault healing. The growing interest in fault healing lies in the fact

that it controls fault stability and the seismic versus aseismic behavior (Ruina, 1983; Tse and Rice, 1986), and the mode of rupture propagation, crack-like or slip-like (Perrin et al., 1995).

Fluids play a key role in fault zones, as proven by the many structural markers found on exhumed faults (veins, stylolites, mineralogical differentiation) or by their high permeability and porosity measured in damage zones after an earthquake (Lockner et al., 2000). The role of fluids during the seismic cycle and their effects on healing processes (see Hickman and Evans, 1995 for a review) is thus crucial. On the one hand, an increase in fluid pressure may bring the fault closer to failure and control earthquake sequences, as shown, for example, for the 2004 Mid-Niigata Prefecture sequence in Japan (Sibson, 2007). On the other hand, fluid-enhanced chemical effects may control fault re-strengthening, these effects including: lithification (Karner et al., 1997; Renard et al., 2000); crack closure (Vidale and Li, 2003); modification of the nature of the contact, from adhesive to welded, due to mineral precipitation (Fredrich and Evans, 1992; Tenthorey and Cox, 2006); increased contact surface area either due to creep (Nakatani and Scholz, 2004; Yasuhara et al., 2004, Goldsby et al.,

* Corresponding author at: ISTerre, University of Grenoble I, CNRS, BP 53, 38041 Grenoble, France.

E-mail address: francois.renard@ujf-grenoble.fr (F. Renard).

2004; Gratier et al., 2009) or to surface tension driven prop growth (Beeler and Hickman, 2004; Hickman and Evans, 1991), and fracture sealing (Boullier et al., 2004). Healing and sealing processes also control the evolution of the permeability of fractures and their ability to transport fluids and transmit pressure in the crust (Matsuki et al., 2001; Polak et al., 2003).

Marone et al. (1995) estimated healing rates or equivalently the strengthening rate from the stress drop variations of small repeating earthquakes as a function of recurrence time intervals. They showed that the stress drop presents a logarithmic growth with time, and that the fault strengthens at a rate in the range 1–3 MPa per decade of time. Such logarithmic time dependence therefore controls the rate of healing of the fault (Beeler et al., 1994).

Similar time dependence appears in laboratory friction experiments, where it is measured, during slide-hold-slide tests, that the pull-off force to slide over an interface increases with the logarithm of hold time (Rabinowicz, 1958, 1995). This ageing behavior is almost universal, as it was observed in laboratory experiments for metals (Rabinowicz, 1995), rocks (Dieterich, 1972), ceramics (Dieterich, 1978), polymers (Bureau et al., 2002), and glass (Berthoud et al., 1999). This frictional healing is attributed to the time-dependent growth and strengthening of contact points (Rabinowicz, 1995; Dieterich, 1972; Dieterich and Conrad, 1984). Some of these experiments were performed at high normal stress, relevant to natural conditions, others at low normal stress. In all cases, healing of the interface was observed. Because friction is proportional to the area of real contacts (i.e. asperities), the healing process can be separated, for each contact, into two effects: increase of the surface area itself and increase of the adhesion (i.e. the strength of the contacts). The asperity surface area is determined by the yield stress of the material and the solid flattens at an asperity so that the normal stress does not exceed this yield stress. The increase of adhesion is mainly dependent on the chemistry of the two solids and on the micro-roughness of the contacts.

The healing effect is included in rate-and-state friction laws. These laws describe the evolution of the friction coefficient μ which depends on the velocity of the slider V and a state variable θ that takes into account memory effects (Dieterich, 1979; Ruina, 1983). Accordingly, friction can be described as

$$\mu(V, \theta) = \mu_0 + a \ln\left(\frac{V}{V_0}\right) + b \ln\left(\frac{V_0 \theta}{D_c}\right) \quad (1)$$

where μ_0 is the friction coefficient for a reference velocity V_0 , D_c is a characteristic distance, and a and b are material dependent empirical constants. In this equation, the last term on the right hand side represents the memory effect due to hold periods or the previous sliding velocity in the case of velocity-stepping experiments. This is described by the state variable θ that can follow at least two different evolution laws, either to take into account slip-dependent strengthening or the time evolution of the contacts (Ruina, 1983). Only the latter law includes an evolution of the friction when the velocity V is equal to zero. In this case (i.e. $V=0$), b scales as the frictional healing rate (Beeler et al., 1994) and thus partly controls the stability of sliding via the value of $(a-b)$ (Scholz, 1998). In the present study, we focus on the experimental rate of frictional healing and study how chemical effects may modify it.

Slide-hold-slide experiments have been reported on bare rock surfaces or simulated fault gouges under high pressure and low or high temperature to estimate healing rate and to infer the physical processes at work (Dieterich and Conrad, 1984; Fredrich and Evans, 1992; Beeler et al., 1994; Nakatani and Mochizuki, 1996; Karner et al., 1997; Blanpied et al., 1998; Karner and Marone, 1998; Mair and Marone, 1999; Frye and Marone, 2002; Nakatani and Scholz, 2004; Yasuhara et al., 2005).

Experiments conducted on simulated gouges of quartz under hydrothermal conditions show higher healing rates after a temperature-dependent cut-off time attributed to pressure solution activation (Nakatani and Scholz, 2004; Yasuhara et al., 2005). Using a soluble rock analog, several experimental results of deformation of salt grains during shear have also confirmed the logarithmic time dependence of healing and the crucial role of grain chemistry and reactivity (Bos and Spiers, 2000; Niemeijer et al., 2008).

Under room temperature and small stress, the static strength of glass-glass interface was investigated (Berthoud et al., 1999) and it was found that, in addition to the logarithmic strengthening, the rate of healing grows with the temperature of the material, and with the state of shear stress applied during the holding periods. Berthoud et al. (1999) have shown experimentally that the level of healing was almost twice larger if the shear stress was maintained constant compared to tests where the shear stress was decreased to zero during the hold period. This was confirmed by Losert et al. (2000) who measured that healing was negligible when no shear stress was applied. Karner and Marone (1998) observed also that, in the absence of shear stress during the hold period, the healing effect could become negative. Note, however, that one study (Nakatani and Mochizuki, 1996) has seen an opposite effect with the healing rate being 10–20% higher when the shear stress was decreased during the hold periods. Finally, transition after some time in the healing rate was observed and attributed to the activation of different healing mechanisms at short and long hold times (Blanpied et al., 1998; Yasuhara et al., 2005; Niemeijer et al., 2008).

The principal purpose of the present study is to analyze which mechanisms may be responsible for the frictional healing of a rock analog interface in presence or absence of chemical reactions and how it modifies the value of the parameter b in Eq. (1). We propose here an analog experiment where we attempt to separate the effects of the various healing mechanisms, and provide some explanation on the wide range of the values of the b parameter found in experimental studies. Hereafter, we investigate the dependence of the strengthening rate of a frictional interface on the chemical reactivity of the two solids in contact. In order to avoid complexities arising from the use of a granular material (i.e. gouge), we work with rough bare surfaces. The reactivity of the interface is controlled by changing the nature of the surfaces in contact (glass/glass; salt/glass; salt/salt) and the fluid (air, water). A camera integrated at the device allows acquiring images of the asperity contacts. The strengthening is derived from the shear force necessary to break the interface and pull-off the slider. It is measured using a force gage. This experimental set-up is built to be analogous to the two surfaces of a natural fracture during the interseismic period and allows characterizing how a macroscopic variable, the strengthening, is controlled by microscopic processes related to contact dynamics.

2. Experimental method

2.1. Friction experiment apparatus

A $1 \times 1 \text{ cm}^2$ surface area slider held under constant normal load, is left in contact with a flat plate (Fig. 1). The slider has a cube shape and is made of either a single crystal of sodium chloride (NaCl) or glass. The 3 cm radius circular flat plate over which the slider is moving is made of either NaCl single crystal or glass. During experiments, the 1 cm^2 nominal surface area of the slider bears a constant normal load of 2.65 kg (0.26 MPa normal stress) imposed by dead weights. The loading rate is controlled by a brushless motor whose speed can vary in the range 0.1–300 $\mu\text{m/s}$.

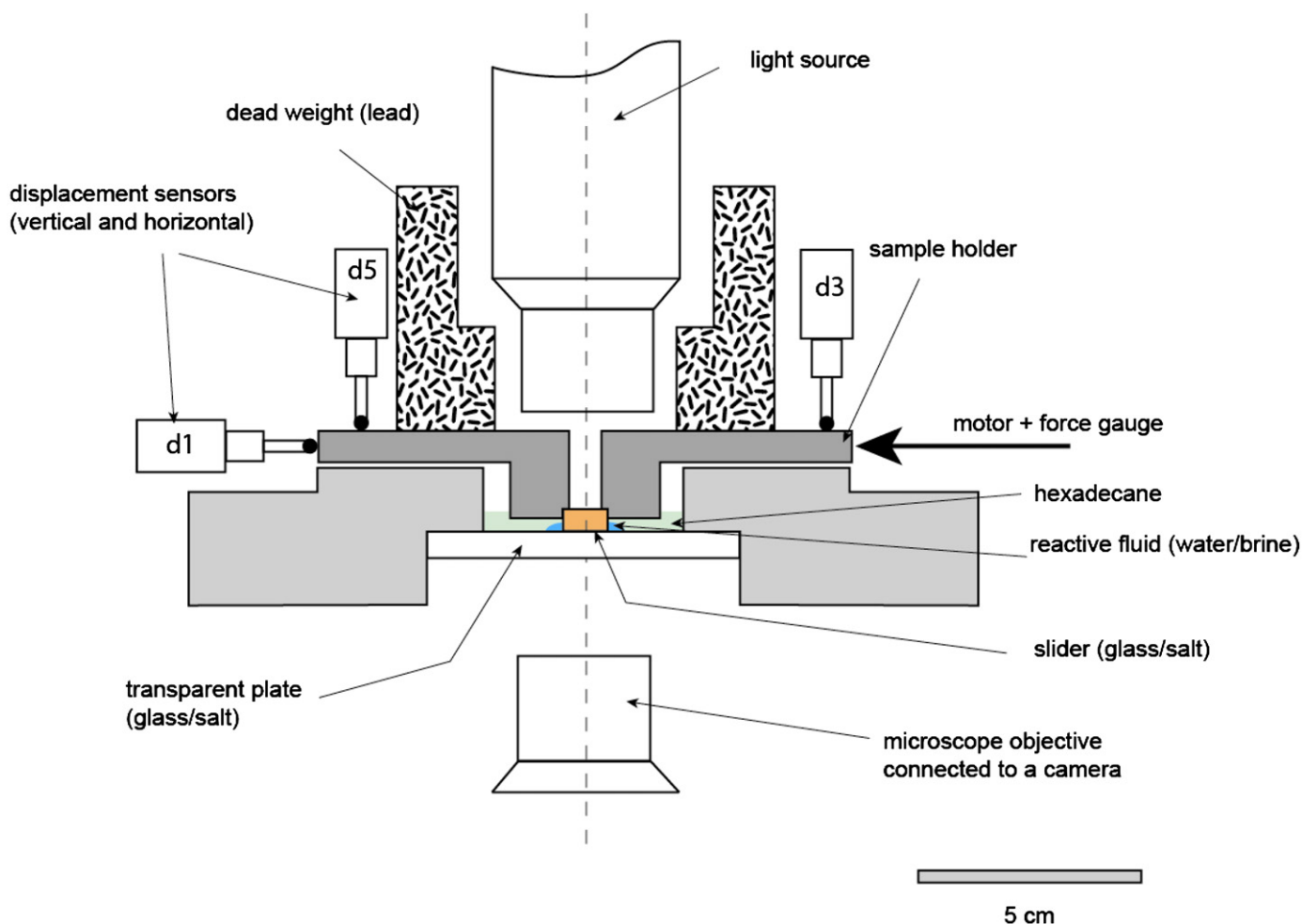


Fig. 1. Experimental friction apparatus to measure the pull-off force of a slider during slide-hold-slide experiments. A slider (salt or glass) is held in a stiff aluminum frame under a constant normal load (dead weight), in contact with a flat plate (salt or glass). Four displacements sensors continuously measure the horizontal (d1) and vertical (d3, d2, d5) displacement of the sample holder (d2 is not shown on this side view). A last sensor (d4) is left away from the experiment on a granite table to measure the noise of the displacement measurements. A 12 bits gray-level camera, connected to the microscope, records the visible evolution of the interface contact asperities with time. For interface strength measurements, a load cell coupled to a motor (arrow) is connected to the sample holder. This ensures a horizontal shear displacement in a direction parallel to the slider/plate interface. Experiments are conducted either at room humidity or in the presence of a reactive fluid. In this last case, a droplet of water or brine is left below the slider, and a film of hexadecane is added to prevent evaporation.

The slide-hold-slide periods are controlled by a Labview® program that also records the data during the tests. The set-up is mounted into a temperature controlled Plexiglas box fixed on a stiff granite table, and located in a temperature insulated dark room. Tests are conducted at 22 °C and the relative humidity of the room, which is not controlled, remains in the range 50–60%. This set-up is a surrogate for the healing/sealing of fractures and faults, where fluid-rock interactions are operative at depth and over the millennium time scale. A similar apparatus was used in Voisin et al. (2007, 2008) and Zigone et al. (2011).

We monitor horizontal and vertical displacements of the slider using four linear variable displacement transducers (Solartron LE/12/S IP50) with sub-micron resolution (Fig. 1). A fifth transducer, left on the granite table, allows characterizing the stability of the displacement measurement, whose standard deviation is equal to 0.1 μm over 24 h. The pull-off shear force necessary to break the interface, allowing the cube to slide again, is measured using a 5 kg force gage sensor (AEP TCA 5 kg) at a sampling frequency of 100 Hz.

The glass surfaces are considered as nominally flat whereas the salt surfaces (slider and flat plate) are textured using sandpaper (Struers, with various grit, see Table 1) to ensure similar initial roughness conditions in all experiments carried out. The glass surfaces are carefully cleaned with acetone and dried before each experiment,

whereas the salt surfaces are cleaned with hexane and then dried. Both surfaces are in equilibrium with the atmospheric humidity.

A slide-hold-slide experiment is composed of a sequence of increasing hold times (ranging from 10 s to 3000 s for most experiments; several tests have also last up to 50 h) separated by slide periods over distances in the range 145–710 μm under an imposed driving velocity (Table 1). During hold periods, the shear stress slowly decreases due to relaxation of the interface (Fig. 2).

2.2. Topography and optical imaging of the interface

For several salt/glass experiments, the contacts at the interface are observed using an optical microscope objective connected to a 12-bits gray levels charge-coupled device camera. Pictures are taken at a frequency of 3 per hour. The topography of several frictional interfaces is also measured before and after the experiments using white light interferometer micro-imaging (Wyko 2000 Surface Profiler from Veeco). In this device, a Michelson interferometer is coupled to a microscope with a broad-band white light source. The interference fringes reach a maximum intensity at equal optical path lengths of the imaging beam and reference beam. By vertical movement of the sample and simultaneous image capturing the interference, we determine the maximum intensity envelope and

Table 1

List of experiments and experimental conditions.

Sample #	Sandpaper grit ^a	Interface	Fluid ^b	Roughness rms (μm)	Loading velocity ($\mu\text{m/s}$)	Sliding distance (μm) ^c	Healing parameter (β)
CREEP008	(S) 320	Salt/glass	Brine	–	no shear	creep	–
CREEP010	(S) 320	Salt/glass	Brine	3.50	no shear	creep	–
CREEP016	(S) 2400	Salt/glass	Brine	–	no shear	creep	–
CREEP018	(C) 0	Salt/glass	Brine	–	no shear	creep	–
CREEP020	(S) 800	Salt/glass	Brine	–	no shear	creep	–
CREEP028	(S) 800	Salt/glass	Brine	–	no shear	creep	–
CREEP045	(S) 320	Salt/glass	Brine	–	no shear	creep	–
S320	(S) 320	Salt/glass	Bare	3.40	–	–	–
S800	(S) 800	Salt/glass	Bare	1.10	–	–	–
S2400	(S) 2400	Salt/glass	Bare	0.70	–	–	–
FR	(S) 320	Salt/glass	Brine	–	35	500	0.0662
DKD1	(S) 320	Salt/glass	Brine	–	35	500	0.0695
DKD2	(S) 320	Salt/glass	Brine	–	35	500	0.0387
DKD3	(S) 320	Salt/glass	Brine	–	35	500	0.0290
Dry	(S) 320	Salt/glass	Dry	–	35	500	0.0355
VVdry2	(S) 320	Glass/glass	Dry	–	14	145	0.0085
VVwet1	(S) 320	Glass/glass	Water	–	14	145	-0.0018
SVdry5	(S) 320	Salt/glass	Dry	–	14	710	0.0204
SVdry20	(S) 320	Salt/glass	Dry	–	68	710	0.0154
SVdry3	(S) 320	Salt/glass	Dry	–	140	710	0.0223
SVdry8	(S) 320	Salt/glass	Dry	–	140	710	0.0207
SVdry21	(S) 320	Salt/glass	Dry	–	140	710	0.0174
SVdry9	(S) 320	Salt/glass	Dry	–	218	710	0.0196
SVdry10	(S) 320	Salt/glass	Dry	–	290	710	0.0164
SVwet1	(S) 320	Salt/glass	Brine	–	14	145	0.0141
SVwet2	(S) 320	Salt/glass	Brine	–	14	145	0.0149
SSdry6	(S) 320	Salt/salt	Dry	–	14	145	0.0306
SSdry1	(S) 320	Salt/salt	Dry	–	14	710	0.0320
SSdry24	(S) 320	Salt/salt	Dry	–	14	710	0.0353
SSdry2	(S) 320	Salt/salt	Dry	–	68	710	0.0231
SSdry22	(S) 320	Salt/salt	Dry	–	140	710	0.0303
SSdry3	(S) 320	Salt/salt	Dry	–	140	710	0.1430
SSdry23	(S) 320	Salt/salt	Dry	–	218	710	0.0190
SSdry11	(S) 320	Salt/salt	Dry	–	14	145	0.0273
SSwet10	(S) 320	Salt/salt	Brine	–	14	145	0.1897

^aC: Castorama sandpaper, S: Struers sandpaper.^bBrine: water saturated with NaCl, dry: atmospheric humidity, water: pure water in equilibrium with the atmosphere, bare: topography measurement of the surface of the slider without deformation experiment.^cCreep: no shear, only uniaxial stress applied to the slider and contact dynamics visualization.

thereby the relative height of the imaged surface at each pixel with a resolution of 3 nm. The horizontal resolution depends on the lens used and with the highest magnification it is at the diffraction limit of white light, of about 0.5 μm . In the present study, we have selected a horizontal resolution of 15.7 μm allowing to image contacts that can reach dimensions of several hundred microns. The height “images” are treated to remove the planar tilt of the surface and fill missing data with linear interpolation. The data obtained is, for each sample, a 2D topographic height field of the slider topography over a selected area. Several striated surfaces were measured before experiments to characterize their initial roughness (samples S320, S800, S1200 in Table 1). Finally, several surfaces were removed from the experimental set-up after healing and observed using a scanning electron microscope for comparison with the white light interferometry images.

2.3. Chemical reactivity of the interface

We conducted three kinds of experiments varying the nature of the interface, the fluid, and thus the chemical reactivity (see Table 1). One series of slide-hold-slide experiments is conducted under ambient humidity with three different interfaces (glass/glass; salt/glass; salt/salt) and is referred to as dry experiments. Note that, under such condition, a thin film of water is absorbed onto the salt surfaces, with a thickness in the micrometer range.

The second slide-hold-slide experiment series is conducted, on the three different interfaces, with water in chemical equilibrium with the solids and is referred to as wet experiments. For these experiments, a droplet of saturated brine (or water for glass/glass interface) is trapped at the interface between the slider and the flat surface. To avoid evaporation, a film of hexadecane covers the sample and the brine, ensuring that it does not penetrate the frictional interface. The third series of experiments is conducted wet, with imposed normal load but without shear stress and for a duration of 50 h and salt/glass interfaces with initial roughness (see Table 1). In these runs, the dynamics of contacts is observed while the salt slider is stationary.

The glass/glass dry interface will be considered as a reference, being *a priori* the less reactive interface. At the other end of the reactivity scale, the salt/salt interface with saturated brine will be considered *a priori* as the most reactive interface.

3. Results

3.1. Slide-hold-slide experiments: effect of surface reactivity on the ageing rate of the interface

Fig. 2 presents a typical record of frictional force during a slide-hold-slide experiment. Here, we define the degree of healing

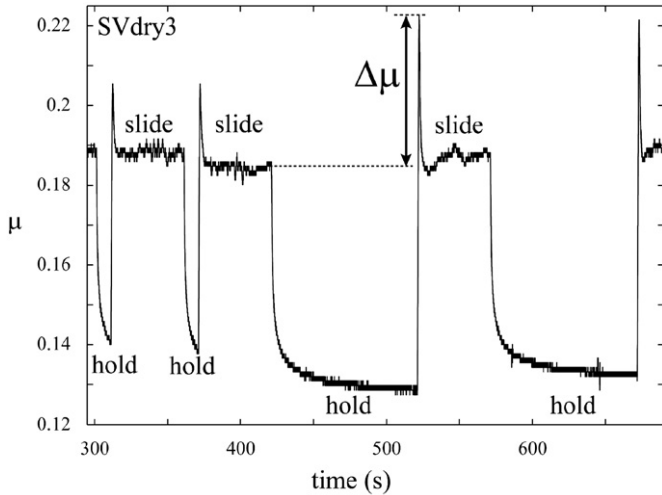


Fig. 2. A typical record of a slide-hold-slide experiment, showing the friction coefficient evolution with time (experiment SVdry3). Experimental conditions: salt/glass interface; normal load of 0.26MPa; temperature of 22 °C; room humidity 50–60%. During the sliding stage, the salt sample is pushed at a loading rate of 10 μm/s during 50 s. During the holding stage, the loading velocity is set to zero and the shear stress slowly relaxes. $\Delta\mu$ is the difference between the peak of static friction after the hold stage and the dynamic friction during the previous sliding stage. It represents a measurement of the healing of the interface.

($\Delta\mu$) as the difference between the peak shear-stress upon re-shear and the preceding steady shear stress normalized by the normal load (as in Marone (1998a) and Niemeijer et al. (2008), for example). In the following, we approximate the healing by the ageing of the interface at rest, and we evaluate how the surface chemical reactivity impacts the healing rate. In order to do so, we vary the nature of the surfaces in contact (salt/salt, salt/glass, glass/glass).

The amount of healing ($\Delta\mu$) as a function of hold time for the six experiments performed with a salt/glass interface in the presence of saturated brine is displayed on Fig. 3. The two plots represent the same data either with semi-logarithmic axes (Fig. 3a) or in a double logarithmic graph (Fig. 3b) and also show the reproducibility of these experiments. For the former case (Fig. 3a), the data may be fitted using a power-law in time, $\Delta\mu \propto t^\alpha$ with a power law exponent $\alpha = 0.24 \pm 0.07$, which was also observed when shearing salt grains (e.g. Bos and Spiers (2002), Fig. 7c). For the latter case (Fig. 3b), the data may be fitted using a logarithmic dependence of time such that $\Delta\mu \propto \beta \log_{10}(1+t/t_c)$ where t_c is a critical time chosen here to be equal to 10 s and a pre-factor $\beta = 0.03 \pm 0.02$. For these two kinds of time dependence, logarithmic or power law with a small exponent, it is quite difficult to differentiate which law is the best fit, particularly because the value of $\Delta\mu$ varies within one order of magnitude only, making it difficult to extract a power law relationship. A better resolution at short times or longer experiments would help discriminate. We note, also, the difficulty to perform long experiments, with the long-term stability required to measure small variations of healing rate. Based on our data, we cannot rule out the power law option. However, for the sake of comparison with previous studies, we will interpret our data using the logarithmic fit later.

In Fig. 4, we have represented the ageing of various interfaces, depending on their chemical reactivity, for hold times in the range 10–3000 s. All data align along different lines in this semi-logarithmic plot, and we characterize ageing as a process that evolves with the logarithm of time to fit these data. In our experiments, the healing rate $\beta = \Delta(\Delta\mu)/\Delta(\log_{10}(t))$ is defined as the slope of the different lines in a semi-logarithmic diagram.

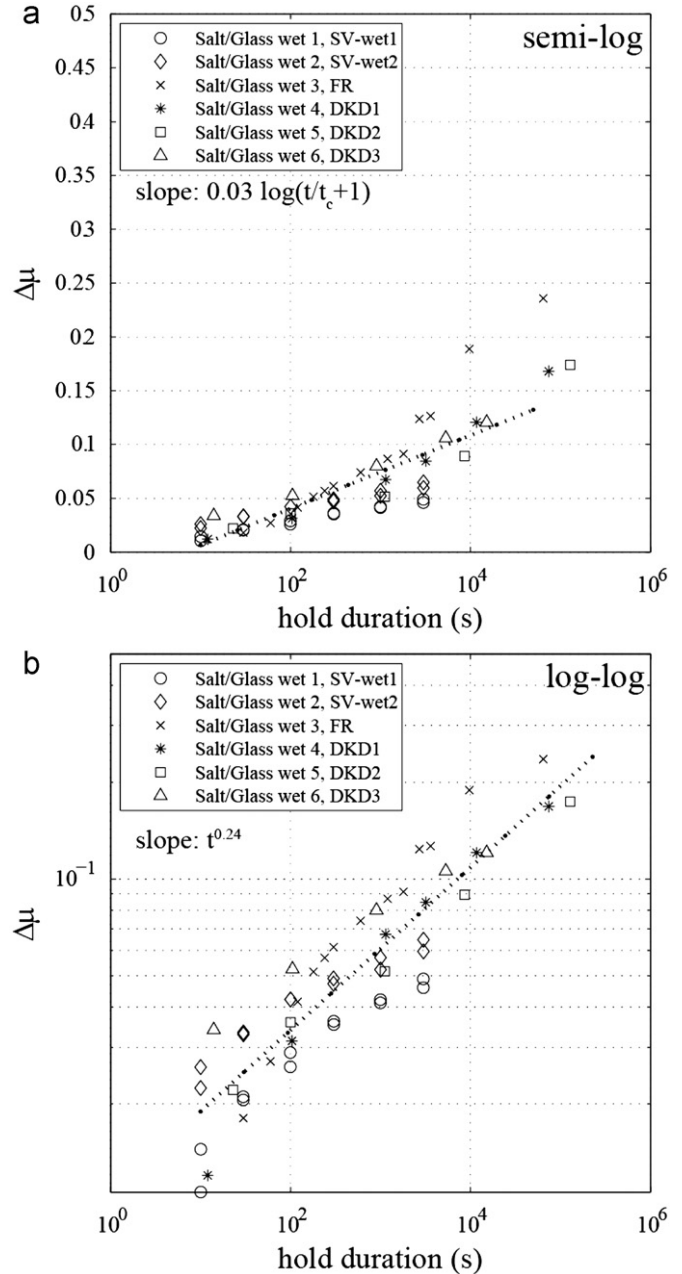


Fig. 3. Healing as a function of hold time for six similar experiments with salt/glass interface in the presence of brine. Two kinds of fit could be considered, either a logarithmic dependence in time (a) or a power law in time (b). These curves also show the reproducibility observed in the experiments. The linear dashed trend represents a fit of all the data and the functional dependence of this fit is given on each plot.

The glass/glass wet case does not exhibit any ageing with time and β is even slightly negative. This is probably due to the lubricating effect of water that prevents the ageing of the interface. This effect is removed when the glass/glass dry case is considered where β is close to 9×10^{-3} . This value can be used as a reference for comparison with the other interfaces. A small jump in the healing rate arises when the salt/glass case is considered where β is close to 1.5×10^{-2} , with or without the presence of fluids, which makes a two folds increase in β . The salt/salt interface in dry condition has a healing rate β close to 3×10^{-2} , which makes a three folds increase. When saturated brine is added, the slope of the ageing evolution is 0.19, six times larger than the salt/salt dry interface, and thirteen times larger

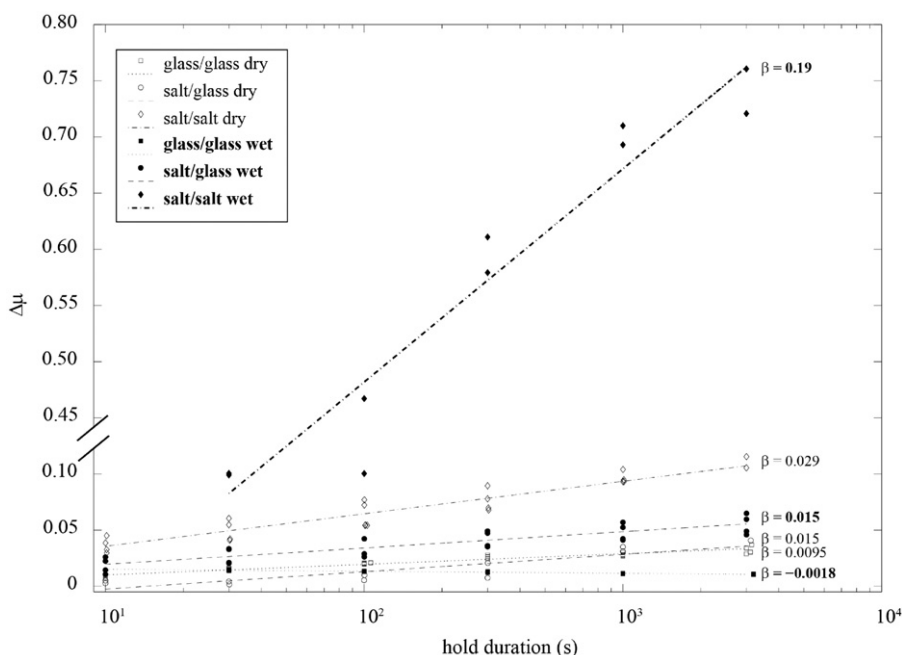


Fig. 4. Effect of chemical reactivity on the healing rate: $\Delta\mu$ as a function of hold time for experiments with different interfaces and humidity conditions: salt/glass dry; salt/glass wet; salt/salt dry; salt/salt wet. Experimental conditions: pressure $P=0.26$ MPa; temperature $T=22$ °C; loading rate $14 \mu\text{m/s}$ over $100 \mu\text{m}$. The hold times range over 2.5 orders of magnitude. For the different experiments, the measurements of $\Delta\mu$ align along straight lines, which indicate an ageing of the interface with the logarithm of time, consistent with previous studies. Differences arise and the various values of the healing rate β are displayed on the figure. We relate the differences in the healing rate to the differences in chemical reactivity at the slider/plate interface.

than the salt/glass wet interface. The healing rate between the two ends of our reactivity scale (dry salt/glass interface and wet salt/salt interface respectively) is increased by more than twenty folds. The healing processes are thus more efficient when two reactive interfaces are in contact and even more in presence of fluids.

Finally, we also note a difference in the sliding behavior; in all experiments except for the salt/salt wet interface the sliding is stable. For the latter interface, without changing any parameters, only by adding a fluid, the sliding becomes highly unstable with a strong stick-slip behavior. This means that on the one hand, even during the slide period, most of time the slider is at rest; on the other hand the healing becomes effective at a level where it affects the stability of sliding.

3.2. Slide-hold-slide experiments: effect of the loading velocity on the healing rate

We focus here on salt/salt and salt/glass dry interfaces and investigate the role of the loading velocity on the healing rate. On Fig. 5 is displayed the evolution of the healing rate for salt/glass and salt/salt interfaces as a function of holding time, for different loading velocities during the sliding periods. As previously seen (Fig. 4), healing increases with holding time. For the salt/glass interface, no systematic effect of the sliding velocity can be seen on the value β (Fig. 5a). However, for a salt/salt dry interface, β clearly varies with sliding velocity; the slower the loading velocity, the higher the healing rate. The inset of Fig. 5b represents this change in the healing rate with V and the dependence of the healing rate with the sliding velocity is linear. Note that the dynamic friction coefficient (shear resistance when sliding) is similar for both interfaces and does not vary significantly with velocity (Supplementary material, Fig. S2). For salt/salt wet conditions, this behavior cannot be investigated because of the presence of stick-slip behavior for which the measurement of a constant sliding velocity is not possible.

3.3. Hold (no slide) experiments: imaging the dynamics of contact asperities

The evolution of the geometry of contact asperities between the two surfaces with time controls the evolution of the strength of the interface and therefore its healing rate. To characterize the contact growth during hold periods, we have performed a series of salt/glass experiments where a constant normal load was applied on the slider, without imposed shear stress or displacement (experiments referenced as “creep” in Table 1). Only the vertical settlement of the slider was followed and the surface area of individual contacts was imaged with the camera at times intervals of 20 min. For dry experiments, the contacts exist, evolve and cover much less than 1% of the whole surface area of the slider, making it difficult to image them through time given the camera resolution. When a droplet of brine is present at the interface, the rich dynamics of salt-fluid interactions allow contact points to grow with time (Fig. 6). These contacts first nucleate at various times, and then start to expand laterally; covering almost 10% of the nominal contact surface area after 20 h for a salt/glass interface.

Individual contact points are initially dispersed over the interface and grow independently (Fig. 6a). Their growth rate is non-linear in time. Moreover, when two contact asperities grow simultaneously close to each other and coalesce (Fig. 6b), the growth rate increases by abrupt steps (Fig. 6c). Using time-lapse images of the same portion of the surface area, the complex time evolution between individual contact nucleation, growth, and merging can be characterized (Fig. 6d).

Both white light measurements and scanning electron microscopy images clearly show that these contacts grow as flat asperities in the open space between the salt slider and the glass plate (Figs. 7 and 8). They initiate on actual contacts that widen in time by several tens of micrometers. SEM images show that the actual contacts are flat, and are either almost circular or show a linear trend when controlled by the initial linear striations of the

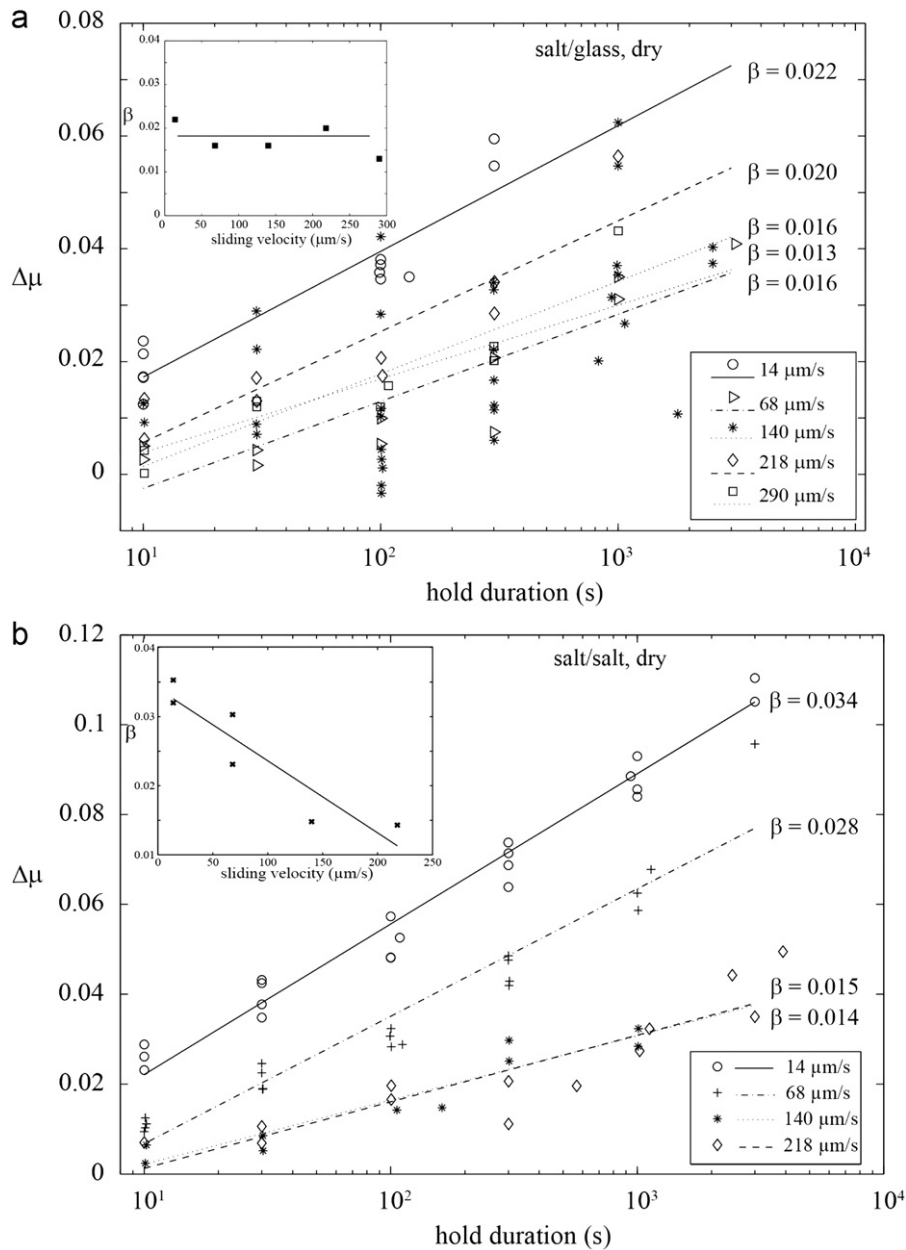


Fig. 5. (a) $\Delta\mu$ as a function of hold time for experiments at five different sliding velocities on a salt/glass dry interface. No clear trend emerges between the value of β and the sliding velocity (see inset). (b) $\Delta\mu$ as a function of hold time for experiments at four different sliding velocities on a salt/salt dry interface. Experimental conditions: normal load 0.27 MPa; temperature 22 °C; sliding distance 500 μm . The lines fit the data with a least square method for each velocity. The slopes of the lines indicated on the right side correspond to the healing rates β . The inset shows how β decreases with loading velocity imposed during the slide stage. The line serves as a guide for the eyes.

surface (Fig. 7c and d). Some of these contacts have formed by merging different smaller contacts (Fig. 7b, e and f).

The white light interferometry data allow for a comparison of the topography of the nominal contact before and after healing. The initial roughness (Fig. 8c) shows almost Gaussian height distribution with a standard deviation close to 5 μm , controlled by the initial polishing of the salt surface with sandpaper. After healing, the roughness distribution becomes bimodal, with a first peak corresponding to the remnants of initial roughness, and a second peak, located at 8.6 μm above the first one, and corresponding to the actual contacts (red curve, Fig. 8c). This second peak is very narrow and shows that the actual contacts are almost flat.

In the mean time, the vertical settlement of the slider is rather small (Fig. S1a), less than 4 μm for most of the experiments.

This demonstrates that, for salt/glass wet interfaces, the contacts grow mainly by a lateral extension, without a clear correlation with the vertical displacement of the slider (Fig. S1b). Therefore, the growth of the contact surface area, at these conditions, is not due to a ductile flattening of existing asperities. This is also observed for glass/glass wet interfaces. This growth process is not observed for dry salt/salt and salt/glass interfaces, indicating that a dissolution-crystallization process, enhanced by the presence of a reactive fluid, may be responsible for the observed fast contact growth.

The healing of salt/salt interfaces with adsorbed humidity or fully saturated is clearly and fundamentally different. A possible explanation is that, with a free fluid, the dissolved salt can be transported on contact to another and therefore even small differences in contact diameter will enhance a maturation of the

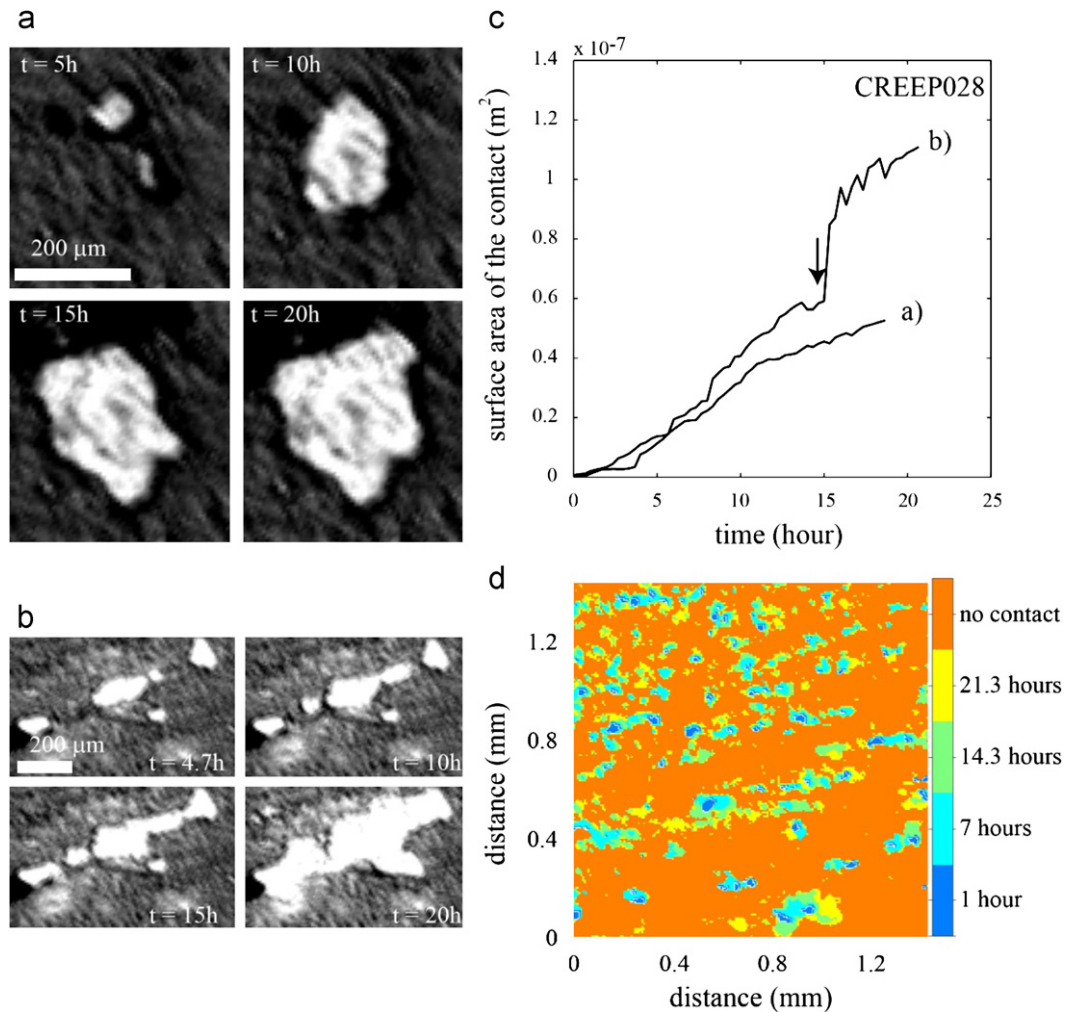


Fig. 6. Time evolution of contact asperities (experiment CREP028). (a) Growth of a single contact with time. (b) Growth of several contacts that merge after $\sim 15\text{ h}$. (c) Evolution of the surface area for the two contacts shown in (a) and (b). The arrow points to the time when the sudden merging of several small contacts occurs. (d) $1.4 \times 1.4\ \text{mm}^2$ time-lapse zoom on the nominal contact area during growth of asperities. The color coding underlines the different times during contact growth and merging. Orange color corresponds to contact-free surface.

interface (i.e. Ostwald ripening and nucleation of new contacts). Conversely, with adsorbed humidity, local mass transfer operates mainly at the scale of a single contact.

Using the nominal contact surface area of Fig. 6d, fifteen individual contacts were selected and their growth was followed through time. The kinetics of this process is displayed on Fig. 9a and a striking observation is that, for individual contacts, a wide range of growth rates is observed. Even single contacts can grow at quite different rates. For multi-contacts, those whose surface area increases by successive coalescence of smaller contacts, the growth rate shows events of rapid increase. We also display on Fig. 9b (thick line) the average growth rate of these contacts that shows non-linear time dependence. This average growth rate is computed at each time by averaging the actual contacts on a given portion of the contact surface. Some contacts do not grow anymore but are still used in the average because they can coalesce with another contact at any time.

4. Discussion

We present experimental observations of the healing and strength recovery of a rough interface in the presence of chemical reactions. Our results first confirm that interface chemical

reactivity plays a major role on healing processes by enhancing the rate of asperity growth. Our work furthermore highlights the key role played by reactive fluids in the dissolution–crystallization processes responsible for the strengthening of the interface, which is attributed here mainly to neck growth of contact asperities and an increase of adhesion by welding of contacts, with only a minor effect of the deformation of asperities by creep. Note also that, in our experiments, the lubricating effect of a continuous water film can be seen on the similar effect of brine on salt/glass and glass/glass interfaces in Fig. 4. This reduces the observed healing rate.

In this discussion section we first compare our results with previous studies. Then we analyze the time-dependence of contact asperity growth (Fig. 9) and we propose a conceptual framework to describe the various mechanisms at work during interface healing (Fig. 10).

4.1. Comparison with previous experimental studies

Healing of salt at room temperature could be due to several processes. On the one hand plastic creep of asperities, either through the motion of defects (Brechet and Estrin, 1994; Dieterich and Kilgore, 1994, 1996) or through a stress-enhanced solution transfer process (Nakatani and Scholz, 2004), could reshape the

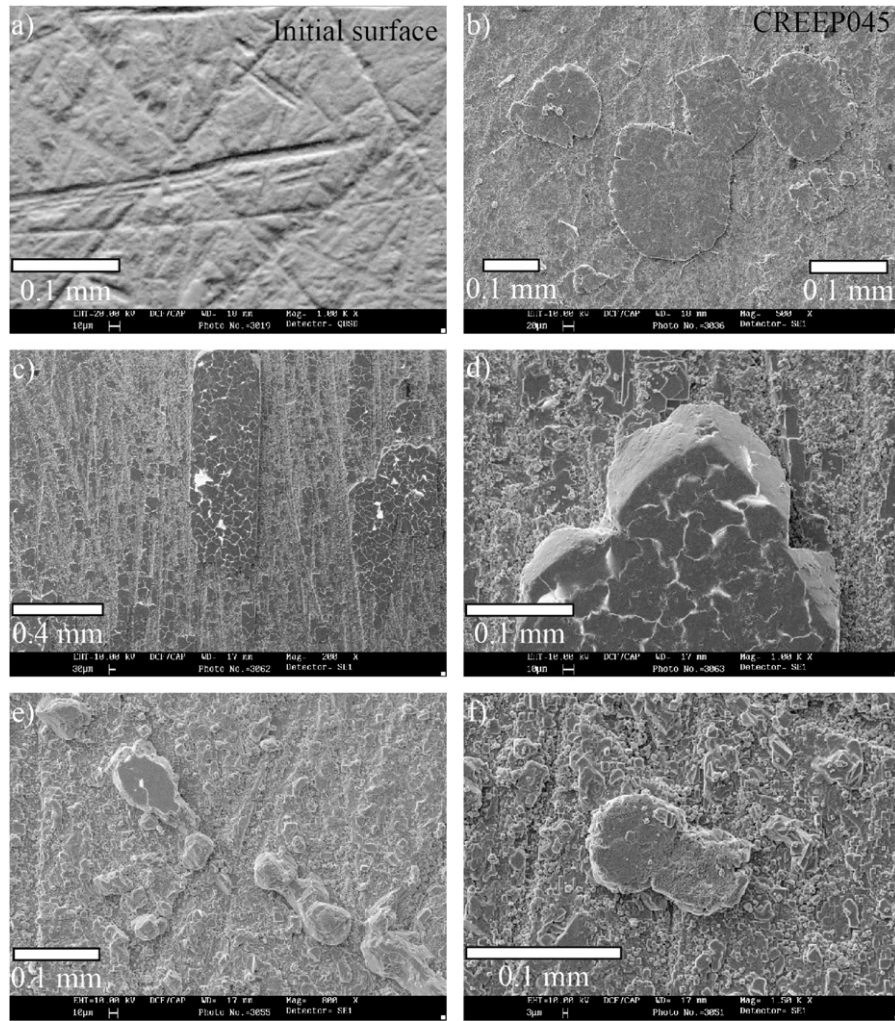


Fig. 7. Scanning electron microscopy images of contacts for a salt/glass interface (experiment CREEP045). (a) Initial surface showing the striations due to polishing. (b–f) Contacts for a salt/glass interface after 24 h of growth. The asperities are planar structures, in contact with the glass plate. When dispersed (c, f), they grow independently. Or they can merge when located close to each other (b, e).

actual contacts and flatten them (Sleep, 2006). On the other hand, subcritical crack growth could also damage these contacts. Hickman and Evans (1991) raised also the possibility that contact neck growth causes the time-dependent healing observed in friction. They showed that the radius of halite–halite contacts grows as $t^{1/4}$ to $t^{1/3}$, an exponent close to the power law fit with $\alpha=0.24 \pm 0.07$ shown on Fig. 3b and to the growth of contacts under stress during pressure solution creep experiments on salt crystals (Dysthe et al., 2002).

Other experimental studies have observed logarithmic dependence in time. The value of the healing parameter β was measured using different geometries – sheared granular materials (i.e. gouge) or bare surfaces – and interpreted in terms of physical processes at the contact scale (see Table 2 for a list of values for β). Blanpied et al. (1998) showed that, when shearing a quartz gouge, the friction coefficient was increasing during hold periods, and that this increase was larger at higher temperatures and in the presence of water as a reactive fluid. By compacting a gouge made of particles of salt mixed with kaolinite clays, Bos and Spiers (2000) observed that the healing rate during hold periods strongly varied if either only halite was present, or mixed with kaolinite. The parameter β was 0.27 for halite gouge and decreased to 0.03 for a mixed gouge. This was interpreted by the effect of clay particles, trapped at halite–halite grain boundaries that prevent contact adhesion and neck growth. Note that these values are

very similar to what is observed in our experiments, with $\beta=0.19$ for a salt/salt interface and $\beta=0.029$ for a salt/glass interface (see Table 2 and Fig. 4). Niemeijer et al. (2006, 2008) used salt gouge as a crustal fault rock analog, at ambient conditions of pressure and temperature. They showed that healing is 10 times faster in wet conditions (saturated brine) than in dry conditions. These results are strongly dependent on the nature of the gouge (salt, salt and phyllosilicates) and on some physical parameters such as grain size and porosity (Niemeijer et al., 2008). Note again that these results are in good agreement with our observations: the healing is more than 6 times faster in wet conditions than in dry conditions for a salt/salt interface; this factor strongly depends on the type of interface.

Nakatani and Scholz (2004) proposed a model of healing where asperities in contact flatten with time due to local creep. This increases the total surface area of contact and also the pull-off force necessary to slide past the interface. In this model, based on Bowden and Tabor (1954) analysis and Brechet and Estrin (1994) model of dynamic friction in metals, the logarithmic dependence of healing in time can be related to the exponential dependence between the strain rate at asperities and stress. Such exponential dependence is also proposed for deformation of minerals by the mechanism of pressure solution creep (Weyl, 1959; Rutter, 1976). In our experiments, scanning electron microscopy and white light interferometry imaging indicate that

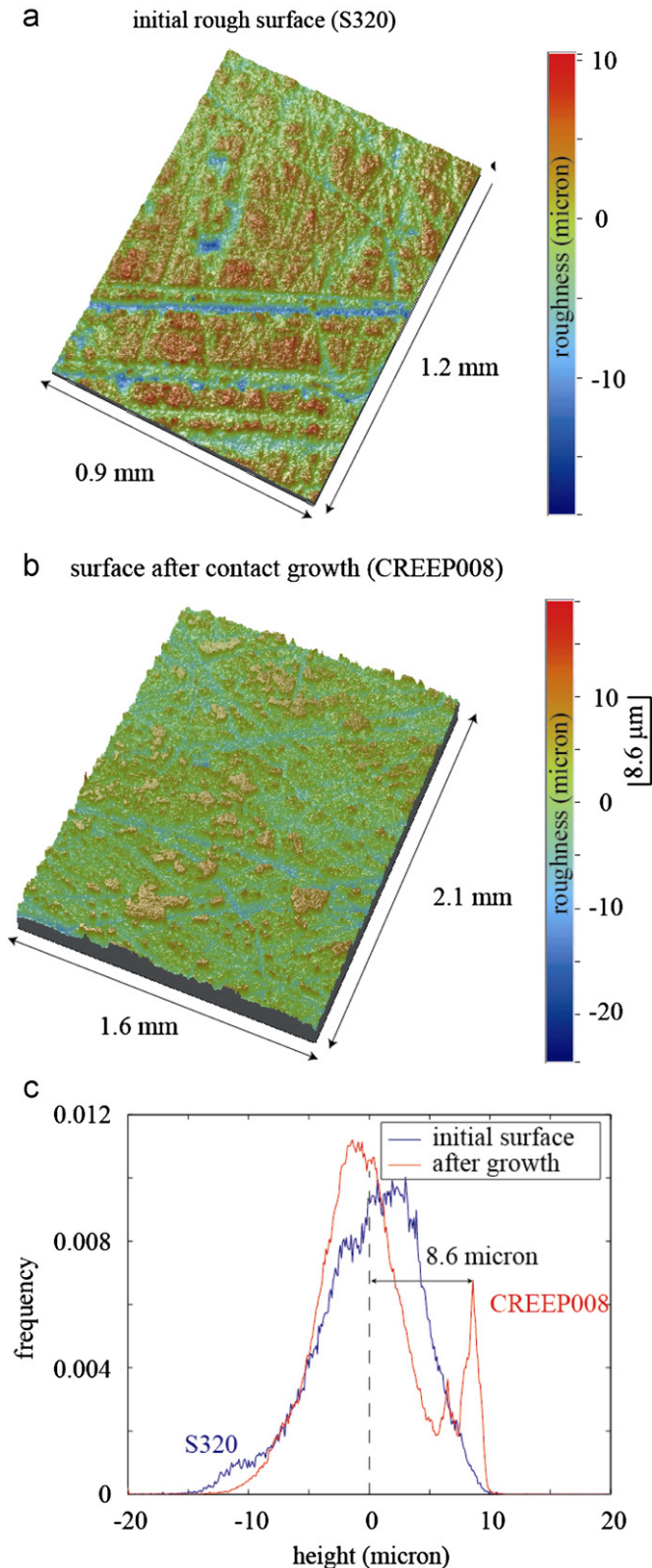


Fig. 8. Geometry and topography of the contact asperities on a salt slider (salt/glass interface). (a–b) White light interferometry roughness measurement of an initial NaCl surface (textured with sandpaper #S320) and of sample CREEP008 after 50 h of contact growth. The contacts correspond to flat asperities located 8.6 μm above the average rough surface. The zero height corresponds to the mean plane of the surface. These two images correspond to different samples. (c) Histogram of the roughness elevation measured using white light interferometry before and after contact growth. The contact appears as a second peak in the height distribution, located 8.6 μm above the average surface.

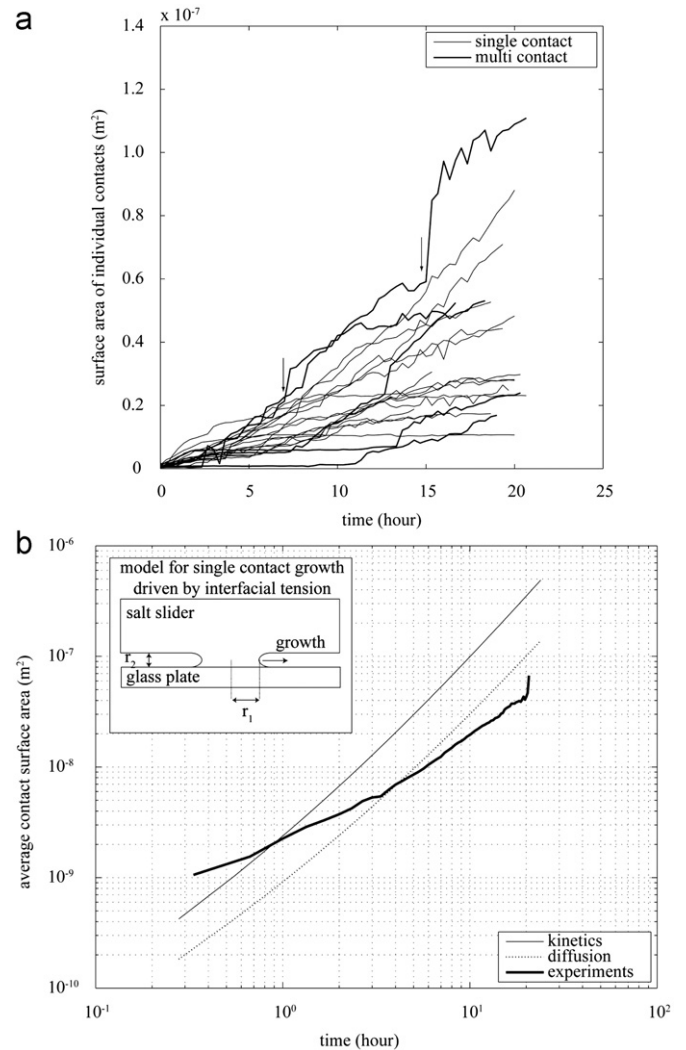


Fig. 9. (a) Surface area $A(t)$ as a function of time of fifteen individual contacts from the interface displayed in Fig. 6d (experiment CREEP008). Multi-contacts (thick lines) grow by connecting individual asperities, which induces more irregular growth. Arrows indicate, for one multi-contact, periods of coalescence with other contacts and sudden surface area growth. (b) Log–log representation of the average growth of asperities. The thick line is an average of the contacts presented in a). Note that the contacts that have stopped growing are still taken into account in the average because we are characterizing the global process of growth. A contact can for example coalesce with another contact and thus participate in the healing behavior on the interface. The two thin lines present models of growth of salt contact driven by interfacial tension and whose rate is limited either by the kinetics of precipitation (plain line, see Eq. (3)) or the kinetics of diffusion (dashed line, see Eq. (4)). The inset shows the geometry of contact growth used.

neck growth mediated by the large curvature across the interface is a plausible mechanism for contact growth (Figs. 6–8). In the following, we examine if a model of healing by neck growth could describe our observations.

4.2. Neck contact growth driven by surface tension versus creep

In our hold experiments (hold with normal stress, without shear displacement) we measured the vertical displacement rate due to the normal stress and we found that it remains much too small (Supplementary material, Fig. S1a) in order to explain the increase of the surface area of the asperities. Asperity deformation may be accommodated by plastic deformation (Fig. 10a). It may also be accommodated by pressure solution creep with mass transfer from dissolution interfaces to the pore space (Fig. 10b).

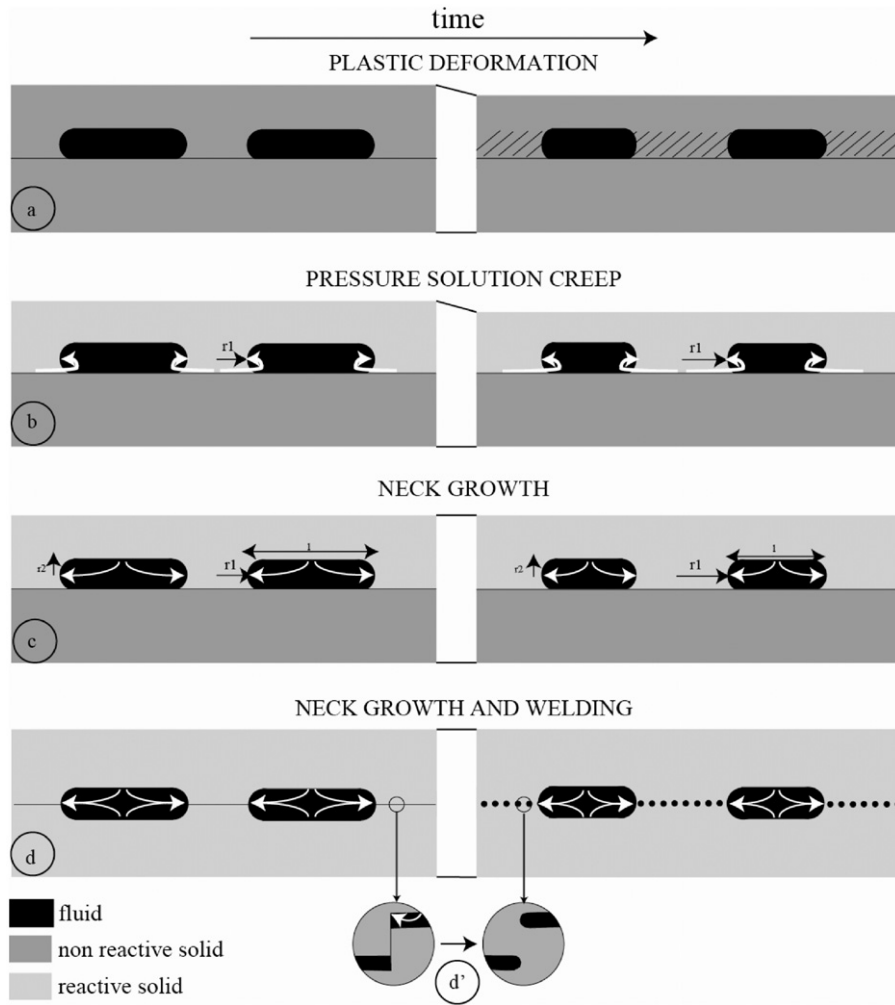


Fig. 10. Mechanisms of healing and strengthening of a frictional interface. (a) Strengthening by plastic deformation of the solid contacts (note the shortening perpendicularly to the interface). (b) Deformation of asperities by pressure solution creep, with dissolution and mass transfer. (c) Neck contact asperities growth driven by minimization of surface energy. (d) Welding and neck growth of contact asperities driven by minimization of surface energy. (d') Mechanism of welding at the contact surface with formation of a network of fluid inclusions.

None of these mechanisms seems to have a major effect in our experiments. Conversely, scanning electron microscopy and white light interferometry imaging indicate that neck growth mediated by the curvature variation across the interface is a plausible mechanism for contact growth (Fig. 10c and d).

The growth of a single contact mediated by the local increase of surface free energy can be described using a simple kinetics model. We consider a contact of radius r_1 and height r_2 (corresponding to the mean separation between the slider and the glass plate), see inset in Figs. 9b and 10c. At the contact edge, the surface tension is smaller than for a flat interface, and the chemical potential difference $\Delta\mu_G$ with a flat interface is

$$\Delta\mu_G = \gamma \left(\frac{1}{r_1} + \frac{1}{r_2} \right) \quad (2)$$

where γ (J m^{-2}) is the interfacial tension energy between sodium chloride and glass (salt/glass interface) or the surface energy to break sodium chloride (salt/salt interface). In the experiments, the contacts growth process decreases the surface energy: a fluid–solid interface is replaced by a solid–solid interface as the contacts expand (Fig. 10c).

To estimate the growth rate of the contacts, we can consider two end-member cases. Either the growth may be controlled by the diffusion of solutes towards the contacts, or it is controlled by

the kinetics of surface reaction, *i.e.* attachment of Na^+ and Cl^- ions at the contact surfaces. If the diffusion length is small enough, the growth rate of the contact is governed by the following precipitation kinetics law:

$$\frac{\partial r_1}{\partial t} = -k_p \bar{V}_s \left(1 - \exp \left[\frac{-\gamma \left(\frac{1}{r_1} + \frac{1}{r_2} \right) \bar{V}_s}{RT} \right] \right) \quad (3)$$

where k_p is the rate constant for salt precipitation, \bar{V}_s is the molar volume of NaCl, R is the gas constant, and T is the absolute temperature. The term in parenthesis represents the departure from equilibrium (*i.e.* local super-saturation) that drives precipitation and contact growth. Instead, if the growth rate is controlled by diffusion, the contact growth law follows:

$$\frac{\partial r_1}{\partial t} = \frac{Dc_{eq} \bar{V}_s}{\delta} \left(1 - \exp \left[\frac{-\gamma \left(\frac{1}{r_1} + \frac{1}{r_2} \right) \bar{V}_s}{RT} \right] \right) \quad (4)$$

Eqs. (3) and (4) can be integrated numerically, starting with an initial contact radius $r_1 = 1.0 \times 10^{-6}$ m (limited by the resolution of our optical observation). Because the rate constant of halite precipitation is not well-known, we have chosen it to be equal to the dissolution kinetics constant measured by Alkattan et al. (1997), $k_p = 2.5 \text{ mol m}^{-2} \text{ s}^{-1}$. The other parameters are the molar

Table 2

Comparison of the values of the healing parameter β in different experiments performed on bare surfaces or granular gouges, for different chemical composition of the solids on each side of the sliding interface.

Sample	μ	$\sigma_{n,eff}, T$	$\beta = A(\Delta\mu) / A(\log_{10}(t))$	References
Salt/salt bare Surf. salt/glass Bare surf. glass/glass bare	0.2 to 0.4	0.26 MPa RT ^a	0.18–0.2 0.01–0.07 0.002–0.01	This study
Salt or salt+kaolinite grains, dry/wet	0.6	2.5 MPa RT ^a	0.27 (pure salt) 0.034 (salt+kaolinite) 0.037 (salt+kaolinite+foliation)	Bos and Spiers (2000, 2002)
Salt+muscovite dry/wet	0.4–0.8	5–10 MPa RT ^a	0.075 (pure salt) 0.1–0.28 (salt+brine) 0.06–0.14 (salt+muscovite)	Niemeijer et al. (2008)
PMMA or PS bare surface, dry ^b	0.4	625 kPa 25–125 °C	0.01 (25 °C) 0.12 (close to melting temperature)	Berthoud et al. (1999)
Granite, bare surface, dry	0.7–0.8	5 MPa RT ^a	0.01–0.03	Nakatani and Mochizuki (1996)
Quartz/alumina grains, dry/wet	0.65	25 MPa RT ^a	0.006 (β increases with relative humidity)	Frye and Marone (2002)
Granite/quartzite bare surface, dry		25 MPa RT ^a	0.013–0.022	Beeler et al. (1994)
PMMA/glass bare surface, dry ^b	0.15	5.5 kPa RT ^a	0.003–0.015	Bureau et al. (2002)
Glass grains against acrylic plate, dry/wet	1–1.15	61 Pa RT ^a	0.003(wet) 0.006 (dry) 0 (shear stress is removed during hold periods)	Losert et al. (2000)
Quartz grains, dry	0.6	25 MPa RT ^a	0.005–0.02	Marone (1998a)
Quartz grains, dry	0.6	25 MPa RT ^a	–0.01 (shear stress is removed during hold periods)	Karner and Marone (1998)
Silica grains, wet	0.7	5 MPa 20–65 °C	0.0041–0.026	Yasuhara et al. (2005)
Quartz grains, wet	0.65	25 MPa RT ^a	0.003–0.02	Karner and Marone (1991)
Quartz grains, wet	0.65	25 MPa RT ^a	0.0082–0.0086	Marone (1998a)
Quartzite, granite bare surface	0.6–1	1.7 MPa RT ^a	–	Dieterich and Conrad (1984)
Quartz grain, wet	0.6–0.7	50 MPa 100–200 °C	0.010–0.014 (wet) close to zero (dry)	Nakatani and Scholz (2004)
Granite grains dry wet	0.7 to 0.8 0.6–0.7	~400 MPa 23–845 °C	0.001–0.1 0.02–0.05	Blanpied et al. (1998)
Quartz grains, wet	0.6–0.7	25 MPa 230–636 °C	0.08–0.1 ^c	Karner et al. (1997) Fredrich and Evans (1992)

^a RT: room temperature.

^b PMMA: poly(methyl methacrylate); PS: polystyrene.

^c Here, the healing rate was calculated from the evolution of the peak friction coefficient.

volume of NaCl $\bar{V}_s = 2.7 \times 10^{-5} \text{ m}^3 \text{ mol}^{-1}$, the solubility of the solid at equilibrium at room temperature $c_{eq} = 5416 \text{ mol m}^{-3}$, the interfacial tension $\gamma = 0.05 \text{ J m}^{-2}$ (Mersmann, 1990), the temperature $T = 295 \text{ K}$, the gas constant $R = 8.32 \text{ J mol}^{-1} \text{ K}^{-1}$ and $r_2 = 8.6 \times 10^{-6} \text{ m}$, which is estimated as the average opening of the interface, see Fig. 8c and the inset in Fig. 9b. We also consider that the mean interface aperture r_2 remains constant in time, which is demonstrated by the vertical displacements showing that the block compacted by an amount significantly smaller than the value taken for r_2 (Supplementary material, Fig. S1). Finally, the diffusion length $\delta(m)$ is taken equal to r_2 and the diffusion coefficient of sodium and chlorine ions in water is $D = 2 \times 10^{-9} \text{ m}^2/\text{s}$.

Eqs. (3) and (4) present two limiting cases of growth of a contact, where the interfacial tension drives the departure from equilibrium. Because of their high curvature, the growth of new salt/glass surfaces decreases the overall energy of the interface. The kinetics of this growth process is displayed on Fig. 9a where the growth rates of contacts measured on a single salt/glass experiment are presented. By averaging the growth of fifteen contacts displayed on Fig. 9a, a master curve (Fig. 9b) shows that, with relevant thermodynamic and geometric parameters for contact growth driven by interfacial forces, the rate increases

non-linearly with time and falls in the range predicted by the rate laws of Eqs. (3) and (4). The main limitation of these simple analytical solutions is that they do not take into account the various times of contact nucleation nor the complexity of the rough interface with local variations of the interface aperture r_2 .

4.3. Effects of shear load and sliding velocity

Several studies have focused on the relation between the shear stress level during the hold stage and the healing rate. Nakatani and Mochizuki (1996) showed an increase by a factor of 2 in the healing rate of bare granite surfaces when varying the shear load. Bureau et al. (2002) obtained similar results for a glass/polymer interface: when the shear stress is reduced during the hold stage, the healing rate is twice less compared to hold stage at the jamming shear stress level. In our experiments, the shear stress level at the beginning of the hold period is imposed by the loading velocity during the previous slide period. Therefore, a change in the driving velocity is immediately turned into a change in the stress level and affects the healing rate.

In our experiments, the effect of sliding velocity on healing is observed only for a salt/salt dry interface (e.g. Fig. 5b): the healing

rate is divided by 2 while the sliding velocity, derived from recording displacement of the slider, increases by a factor 20. The effect is not observed for a salt/glass dry interface (inset in Fig. 5a). In a velocity-weakening material, the dynamic friction decreases with the logarithm of the step in sliding velocity. Previous studies in literature report an increase of the healing with the velocity, consistent with a velocity-strengthening behavior (e.g. Marone, 1998a, 1998b). Moreover it appears that the dependence of the healing rate with the sliding velocity is linear, and thus should be exponential with the shear stress, during hold periods (inset, Fig. 5b).

A possible explanation could be that, in the experiments without reactive fluid, healing is mainly due to plastic deformation (Fig. 10a) and consequently depends mostly on stress. In our experiment, the shear stress remains stored as elastic strain energy at the contacts during the hold period and may prevent healing. This can be explained if healing is time dependent, so if some reactive fluid phase is present at the contacts, even in dry conditions. Stress relaxation may slow the welding or the neck contact growth. It is observed (Fig. 4, and Supplementary material, Fig. S2) that behaviors of dry salt/salt or wet and dry salt/glass interface are not very different. It is possible that a thin absorbed fluid film could be present at the contacts and affects the behavior of the interface even in dry conditions when at least one of the two solid may react with water.

To conclude on this point, in our experiments the shear stress is not controlled independently of the velocity. So changing the sliding velocity implies a change in the shear stress during slide period but also during hold period. Moreover, we record a relaxation of the shear stress during hold time which may explain the evolution of the healing rate with the shear stress. In the experiments with salt, both a and b are of the same order of magnitude (see Voisin et al., (2007) for measurements of a and b in the same experimental apparatus). Consequently, it is difficult to decipher if the amount of shear stress may affect a , b , or both.

This relaxation without fluid may be associated to plastic deformation at the interface that accommodates a part of the shear stress imposed during hold time. Our results thus highlight that the shear stress is one of the driving forces for the healing process active on salt/salt dry interface, the shear stress decreases during hold periods, and the healing rate is negatively correlated to the sliding velocity.

4.4. Evolution of interface strength in faults: effect of healing/sealing mechanisms

At a macroscopic scale, the interface pull-off process due to bond breaking usually does not occur uniformly over the whole fault surface, but occurs by crack propagation through the asperities which pin the rupture along the interface. The local stress at the asperity (i.e. crack tip) is much higher than the average stress acting on the nominal contact area, and this drastically reduces the pull-off force. Our experiments show the presence of various mechanisms at the origin of asperities strengthening: creep (asperity deformation), neck growth (increase of asperity surface area), and welding (increase of asperity strength). We have already mentioned the minor effect of asperity deformation versus neck growth (see Section 4.2). Neck growth of asperities versus welding may be evaluated from salt/salt versus salt/glass experiment. Here, we can separate these different effects by varying the nature of the interface and thus controlling its chemical reactivity. Because the salt/salt interface can weld, this gives an upper boundary for the strength recovery compared to salt/glass interfaces for which strength increase is mainly due to contact surface area growth. The difference of strength between these two systems can be related to the

difference in energy required to create new salt/salt or salt/glass surfaces when breaking the interface. The effect of welding clearly overwhelms the effect of neck growth, the healing rate being 20 times higher when the solids can weld than when they cannot. The mechanism of welding was not especially investigated in our study. It is possible that the same mechanism of surface energy minimization acts at small scale: irregular shape of rough interface, with angular angles (Fig. 10d, left) may evolve to a cloud of fluid inclusions (Fig. 10d, right). Because the kinetics of such process is inversely proportional to the size of the inclusions and to their spacing, the smaller the roughness the higher the healing rate.

Our experiments also show that a large variability can exist between individual asperities growth, with various nucleation times and the possibility of coalescence. All these processes induce a non-linear dependence of the strengthening process on time and demonstrate the importance of chemical effects on its rate. This implies that, for the Dieterich/Ruina like friction laws, the strengthening parameter depends on the chemical nature of the surfaces in contact, and a variety of values could be found. For example, in carbonate faults, with almost pure calcite composition, the welding of the fractures could be very efficient at least at low temperature (first five kilometers depth in the crust), where calcite solubility is maximum. In the same manner in quartzite faults, with almost pure quartz, the welding must occur rapidly at high temperature, where quartz solubility is higher. Conversely, for faults containing clay minerals or phyllosilicates, that would prevent contact welding, the healing rate could be much lower (Bos and Spiers, 2000; Niemeijer and Spiers, 2006). This also indicates that, even without fracture closing and/or compaction, welding is a very efficient mechanism for strength recovery.

Our estimations of healing rate for a bare textured interface are very close to those found for synthetic fault gouges (Niemeijer et al., 2008). The healing rate in laboratory friction experiments shows similarities with the logarithmic time dependence of stress drop for repeating earthquakes (Marone et al., 1995). The strengthening rate of a fault will be similar if the coseismic rupture is localized either on a plane or in a thin layer of crushed rocks (i.e. fault gouge, cataclasite).

Our experiments confirm that fluids have two crucial but competitive roles in fault re-strengthening. On the one hand, a mechanical lubricating effect prevents re-strengthening if a continuous water film is present and may bring the fault closer to failure. On the other hand, fluids enhance chemical effects responsible for fault re-strengthening and delay the time to failure. In our experiments, the competition between these two extreme roles is strongly controlled by the type of materials put in contacts. For an inert material such as glass, fluids play the role of lubricant. For a reactive material such as salt, fluid plays the role of catalyst of chemical reactions. On faults, the nature of rocks but also physical parameters such as grain size, porosity, pressure and temperature control the two key roles of the fluids (Niemeijer et al., 2008). Moreover, in our experiments, fluids are in equilibrium with the materials at the interface, while in fault rocks, it is not always the case.

5. Conclusion

Assessing how an interface may recover strength with time represents a fundamental issue to predict stress evolution in a fault zone during the interseismic period. In the present study, we have monitored the strength evolution of a frictional interface and varied the chemical reactivity of the solids in contact. The strengthening process occurred by the growth of contact asperities with non-linear time dependence, and the increase of

adhesion of the welded contacts. The healing effect is parameterized by a single parameter β , the coefficient of time-dependent strengthening, which varies between almost zero for non-reactive glass/glass interface, to 10^{-2} for glass/salt interfaces where the asperities increased in size by neck growth but did not weld, and β reaches 0.2 for salt/salt interfaces where the increase in strength is due to both contact growth and welding. Depending if welding is possible or not, the healing rate can therefore vary within a factor 20, the welding of contacts allowing a much stronger recovery of the mechanical properties of the interface. The nonlinear time dependence of the strength recovery of a frictional interface is therefore due to a complex interaction between contact surface area growth, nucleation of new contacts, and contact welding, the latter process being responsible for the largest healing rates observed.

Acknowledgments

We thank Pierre Giroux, Liliane Jenatton, and Benjamin Vial, for their technical help and Benoit Derode, Salif Koné, Danitza Planet, and Anne-Marie Boullier for fruitful discussions. The project was funded by the University Grenoble I and the ANR grant JCJC-0011-01.

Appendix A. Supporting information

Supplementary data associated with this article can be found in the online version at <http://dx.doi.org/10.1016/j.epsl.2012.04.048>.

References

- Alkattan, M., Oelkers, E., Dandurand, J.-L., Schott, J., 1997. Experimental studies of halite dissolution kinetics. 1. The effect of saturation state and the presence of trace metals. *Chem. Geol.* 137, 201–219.
- Beeler, N.M., Tullis, T.E., Weeks, J.D., 1994. The roles of time and displacement in the evolution effect in rock friction. *Geophys. Res. Lett.* 21 (18), 1987–1990.
- Beeler, N.M., Hickman, S.H., 2004. Stress induced, time-dependent fracture closure at hydrothermal conditions. *J. Geophys. Res.* 109, B02211, <http://dx.doi.org/10.1029/2002JB001782>.
- Berthoud, P., Baumberger, T., G'Sell, C., Hiver, J.-M., 1999. Physical analysis of the state- and rate-dependent friction law: static friction. *Phys. Rev. B* 59, 14313–14326.
- Blanpied, M.L., Marone, C.J., Lockner, D.A., Byerlee, J.D., King, D.P., 1998. Quantitative measure of the variation in fault rheology due to fluid-rock interactions. *J. Geophys. Res.* 103, 9691–9712.
- Boullier, A.M., Fujimoto, K., et al., 2004. Textural evidence for recent co-seismic circulation of fluids in the Nojima fault zone, Awaji island, Japan. *Tectonophysics* 378, 165–181.
- Bos, B., Spiers, C.J., 2000. Effect of phyllosilicates on fluid-assisted healing of gouge-bearing faults. *Earth Planet. Sci. Lett.* 184, 199–210.
- Bos, B., Spiers, C.J., 2002. Fluid-assisted healing processes in gouge-bearing faults: insights from experiments on a rock analogue system. *Pure Appl. Geophys.* 159, 2537–2566.
- Bowden, F.P., Tabor, D., 1954. *The Friction and Lubrication of Solids*. Oxford University Press.
- Brechet, Y., Estrin, Y., 1994. The effect of strain rate sensitivity on dynamic friction of metals. *Scr. Metall. Mater.* 30, 1449–1454.
- Brenguier, F., Campillo, M., Hadziioannou, C., Shapiro, N.M., Nadeau, R.M., Larose, E., 2008. Post seismic relaxation along the San Andreas fault at Parkfield from continuous seismological observations. *Science* 321, 1478–1481.
- Bureau, L., Baumberger, T., Caroli, C., 2002. Rheological ageing and rejuvenation in solid friction contacts. *Eur. Phys. J. B*, 331–337.
- Dieterich, J.H., 1972. Time-dependent friction in rocks. *J. Geophys. Res.* 77 (20), 3690–3697.
- Dieterich, J.H., 1978. Time-dependent friction and the mechanics of stick-slip. *Pure Appl. Geophys.* 116, 790–806.
- Dieterich, J.H., 1979. Modeling of rock friction 1. Experimental results and constitutive equations. *J. Geophys. Res.* 84, 2161–2168.
- Dieterich, J.H., Conrad, G., 1984. Effect of humidity on time- and velocity-dependent friction in rocks. *J. Geophys. Res.* 89, 4196–4202.
- Dieterich, J.H., Kilgore, B.D., 1994. Direct observation of frictional contacts: New insights from state-dependent properties. *Pure Appl. Geophys.* 143, 283–302.
- Dieterich, J.H., Kilgore, B.D., 1996. Imaging surface contacts: power law contact distribution and contact stresses in quartz, calcite, glass, and acrylic plastic. *Tectonophysics* 256, 212–239.
- Dysthe, D.K., Podladchikov, Y., Renard, F., Feder, J., Jamtveit, B., 2002. Universal scaling in transient creep. *Phys. Rev. Lett.* 89 (24), 246102.
- Frye, K.M., Marone, C., 2002. Effect of humidity on granular friction at room temperature. *J. Geophys. Res.* 107 (B11), 2309.
- Fredrich, J.T., Evans, B., 1992. Strength recovery along simulated faults by solution transfer processes. In: Tillerson, J.R., Waversik, W. (Eds.), *Mechanical Behavior of Crustal Rocks*, 24. American Geophysical Union, Geophysical Monograph, pp. 103–120.
- Goldsbey, D.L., Rar, A., Pharr, G.M., Tullis, T.E., 2004. Nano-indentation creep of quartz, with implications for rate- and state-variable friction laws relevant to earthquake mechanics. *J. Mater. Res.* 19, 357–365.
- Gratier, J.P., Favreau, P., et al., 2003. Modelling fluid transfer along Californian faults when integrating pressure solution crack-sealing and compaction processes. *J. Geophys. Res.* 108, 2104, <http://dx.doi.org/10.1029/2001JB000380>.
- Gratier, J.-P., Guiguet, R., Renard, F., Jenatton, L., Bernard, D., 2009. A pressure solution creep law for quartz from indentation experiments. *J. Geophys. Res.* 114, B03403, <http://dx.doi.org/10.1029/2008JB005652>.
- Hickman, S.H., Evans, B., 1991. Experimental pressure solution in halite: the effect of grain/interphase boundary structure. *J. Geol. Soc. London* 148, 549–560.
- Hickman, S.H., Evans, B., 1995. Kinetics of pressure solution at halite-silica interfaces and intergranular clay films. *J. Geophys. Res.* 100, 13113–13132.
- Karner, S.L., Marone, C., 1991. Frictional restrengthening in frictional fault gouge: Effect of shear load perturbations. *J. Geophys. Res.* 106, 19319–19337.
- Karner, S.L., Marone, C., Evans, B., 1997. Laboratory study of fault healing and lithification in simulated fault gouge under hydrothermal conditions. *Tectonophysics* 277, 41–55.
- Karner, S.L., Marone, C., 1998. The effect of shear load on frictional healing in simulated fault gouge. *Geophys. Res. Lett.* 24, 4561–4564.
- Li, Y.-G., Vidale, J.E., Day, S.M., Oglesby, D.D., Cochran, E., 2003. Postseismic fault healing on the rupture zone of the 1999 m 7.1 Hector Mine, California, earthquake. *Bull. Seismol. Soc. Am.* 93 (2), 854–869.
- Lockner, D.A., Naka, H., Tanaka, H., Ito, H., Ikeda, R., 2000. Permeability and strength of core samples from the Nojima fault of the 1995 Kobe earthquake. In: *Proceedings of the International Workshop on the Nojima Fault Core and Borehole Analysis*, U.S. Geological Survey Open-File Report 00-129.
- Losert, W., Geminard, J.-C., Nasuno, S., Gollub, J.P., 2000. Mechanisms for slow strengthening in granular materials. *Phys. Rev. E* 61, 4060–4068.
- Mair, K., Marone, C., 1999. Friction of simulated fault gouge for a wide range of velocities and normal stresses. *J. Geophys. Res.* 104, 28,899–28,914.
- Marone, C., Vidale, J.E., Ellsworth, W.L., 1995. Fault healing inferred from time dependent variations in source properties of repeating earthquakes. *Geophys. Res. Lett.* 22 (22), 3095–3098.
- Marone, C., 1998a. The effect of loading rate on static friction and the rate of fault healing during the earthquake cycle. *Nature* 391, 69–72.
- Marone, C., 1998b. Laboratory derived friction laws and their application to seismic faulting. *Annu. Rev. Earth Planet. Sci.*, 26.
- Matsuki, K., Wang, E.Q., Sakaguchi, K., Okumura, K., 2001. Time-dependent closure of a fracture with rough surface under constant normal stress. *Int. J. Rock Mech. Min. Sci.* 38, 607–619.
- Mersmann, A., 1990. Calculation of interfacial tension. *J. Cryst. Growth* 102, 841–847.
- Nakatani, M., Mochizuki, H., 1996. Effects of shear stress applied to surfaces in stationary contact on rock friction. *Geophys. Res. Lett.* 23 (8), 869–872.
- Nakatani, M., Scholz, C.H., 2004. Frictional healing of quartz gouge under hydrothermal conditions: 1. experimental evidence for solution transfer healing mechanism. *J. Geophys. Res.* 109, B07202.
- Niemeijer, A.R., Spiers, C.J., 2006. Velocity dependence of strength and healing behavior in simulated phyllosilicate-bearing fault gouge. *Tectonophysics* 427, 231–253.
- Niemeijer, A., Marone, C., Elsworth, D., 2008. Healing of simulated fault gouges aided by pressure solution: results from rock analogue experiments. *J. Geophys. Res.* 113, B04204.
- Perrin, G., Rice, J.R., Gu, J.C., 1995. Self-healing pulse on a frictional surface. *J. Mech. Phys. Solids* 43, 1461–1495.
- Polak, A., Elsworth, D., Yasuhara, H., Grader, A.S., Halleck, P.M., 2003. Permeability reduction of natural fractures under net dissolution by hydrothermal fluids. *Geophys. Res. Lett.* 30, 2020, <http://dx.doi.org/10.1029/2003GL017575>.
- Rabinowicz, E., 1958. The intrinsic variables affecting stick-slip process. *Proc. Phys. Soc.* 71, 668–675.
- Rabinowicz, E., 1995. *Friction and Wear of Materials*, 2nd ed. John Wiley & Sons.
- Renard, F., Gratier, J.P., Jamtveit, B., 2000. Kinetics of crack-sealing, intergranular pressure solution, and compaction around active faults. *J. Struct. Geol.* 22, 1395–1407.
- Ruina, A., 1983. Slip instability and state variable friction laws. *J. Geophys. Res.* 88, 10,359–10,370.
- Rutter, E.H., 1976. The kinetics of rock deformation by pressure solution. *Philos. Trans. R. Soc. London* 283, 203–219.
- Scholz, C.H., 1998. Earthquakes and friction laws. *Nature* 391, 37–42.
- Sibson, R.H., 2007. An episode of fault-valve behavior during compressional inversion? The 2004 M(J)6.8 Mid-Niigata Prefecture, Japan, earthquake sequence. *Earth Planet. Sci. Lett.* 257, 188–199.
- Sleep, N.H., 2006. Real contacts and evolution laws for rate and state friction. *Geochem. Geophys. Geosyst.* 7, Q08102, <http://dx.doi.org/10.1029/2005GC001187>.

- Tenthorey, E., Cox, S.F., 2006. Cohesive strengthening of fault zones during the interseismic period: An experimental study. *J. Geophys. Res.* 111, B09202.
- Tse, S., Rice, J.R., 1986. Crustal earthquake instability in relation to the depth variation of frictional slip properties. *J. Geophys. Res.* 91, 9452–9472.
- Voisin, C., Renard, F., Grasso, J.R., 2007. Long term friction: from stick–slip to stable sliding friction. *Geophys. Res. Lett.* 34, L13301.
- Voisin, C., Grasso, J.R., Larose, E., Renard, F., 2008. Evolution of seismic signals and slip patterns along subduction zones: Insights from a friction lab scale experiment. *Geophys. Res. Lett.* 35, L08302.
- Vidale, J.E., Li, Y.G., 2003. Damage to the shallow Landers fault from the nearby Hector Mine earthquake. *Nature* 421, 524–527.
- Yasuhara, H., Elsworth, D., Polak, A., 2004. Evolution of permeability in a natural fracture: Significant role of pressure solution. *J. Geophys. Res.* 109, B03204, <http://dx.doi.org/10.1029/2003JB002663>.
- Yasuhara, H., Marone, C., Elsworth, D., 2005. Fault zone restrengthening and frictional healing: the role of pressure solution. *J. Geophys. Res.* 23, B06310.
- Weyl, P.K., 1959. Pressure solution and the force of crystallization: a phenomenological theory. *J. Geophys. Res.* 64, 2001–2025.
- Zigone, D., Voisin, C., Larose, E., Renard, F., Campillo, M., 2011. Slip acceleration generates tremor like signals in friction experiment. *Geophys. Res. Lett.* 38, L01315.